Molecular characterization of calreticulin gene in mud crab *Scylla paramamosain* (Estampador): implications for the regulation of calcium homeostasis during moult cycle

Binpeng Xu[1], Chen Long[1], Weiren Dong[2], Qingjun Shao[1] & Miaoan Shu[1]

[1]College of Animal Sciences, Zhejiang University, Hangzhou 310058, China
[2]College of Life Sciences, Zhejiang University, Hangzhou 310058, China

Correspondence: M Shu, College of Animal Sciences, Zhejiang University, Hangzhou 310058, China. E-mail: shuma@zju.edu.cn

Abstract

Calreticulin (CRT), a well conserved endoplasmic reticulum-resident protein for Ca^{2+}-binding, is widely expressed in multicellular eukaryotes. CRT plays a key role in many cellular processes, including Ca^{2+} homeostasis. To address the role of CRT underlying the Ca^{2+} homeostasis alternation during the mineralization cycle of the mud crab (*Scylla paramamosain*), we cloned the full-length cDNA of CRT gene (*SpCRT*) from *S. paramamosain*, and its protein contains all signature domains of CRT. Tissue distribution showed the *SpCRT* transcript was far more abundant in hepatopancreas than in others. Meanwhile, seven moult stages of the crab were characterized by observing the third maxilliped under microscope and clear uropod images were presented. During the moult cycle, the total calcium levels in the hepatopancreas were determined using ICP-AES. It decreased significantly at stage A and B (p 0.05), and was relatively steady between inter-moult C and early pre-moult D_0 (p 0.05). It was then gradually increased thereafter by nearly 274.2% until stage E (compared with stage C) (p 0.05). Additionally, the expression of *SpCRT* in the hepatopancreas was the lowest in the moult stage E and post-moult stage A, and then it maintained at a high level in other stages. Taken together, the relative retard timing of calcium incrument corresponding to the higher expression of *SpCRT* may suggest CRT plays a critical role in Ca^{2+} storage in hepatopancreas during the moult cycle of crustaceans.

Introduction

Moult is fundamental for the growth and reproduction of crustacean. Crab has emerged as a model system for studying the mechanisms of calcium (Ca^{2+}) homeostasis, because the directionality and magnitude of transepithelial Ca^{2+} flux are dramatically regulated during the moult cycle (Wheatly, Zanotto & Hubbard 2002). Specifically, crustaceans exhibit Ca^{2+} balance in inter-moult, transition to net loss in pre-moult associated with cuticular demineralization, and following ecdysis, start to impressive post-moult accumulation to harden the new exoskeleton (Gao & Wheatly 2007). Ca^{2+} is critical to the formation of mineralized tissues, such as bones and cuticles and it stores mainly in the lumen of the ER. Fluctuations of the ER luminal Ca^{2+} concentration affect intracellular Ca^{2+} homeostasis (Bibi, Agarwal, Dihazi, Eltoweissy, van Nguyen, Mueller & Dihazi 2011).

An ideal candidate to modulate Ca^{2+} homeostasis is careticulin (CRT), a key Ca^{2+}-binding/buffering endoplasmic reticulum (ER)-resident protein that is highly conserved and extensively expressed in many organisms investigated (Michalak, Groenendyk, Szabo, Gold & Opas 2009; Lenartowski, Suwinska & Lenartowska 2015). It typically consists of three structural and functional regions: a highly conserved N-domain, a proline-rich P-domain and a very acidic C-domain (Michalak,

Corbett, Mesaeli, Nakamura & Opas 1999). Due to its calcium binding C-domain and accumulation of large amounts of Ca^{2+} without an excessive increase in the free ER intraluminal Ca^{2+} concentration, CRT was proved to regulate the intracellular Ca^{2+} homeostasis and ER Ca^{2+} storage capacity (Michalak *et al.* 2009; Bibi *et al.* 2011). In contrast to the extensive literature on CRT regulation Ca^{2+} homeostasis in mammals and plants (Jia, He, Jing & Li 2009; Michalak *et al.* 2009; Wang, Groenendyk & Michalak 2012; Lenartowski *et al.* 2015), little information is available on the CRT expression to modulate Ca^{2+} homeostasis in crustaceans (Luana, Li, Wang, Zhang, Liu & Xiang 2007). Moreover, a definite connection between calcium variation and CRT expression has yet to be demonstrated in crustaceans.

The mud crab (*Scylla paramamosain*) is a commercially important aquacultural crustacean due to its fast growth and good flavour (Yeh, Chiu, Shiu, Huang & Liu 2014). The *Scylla* genus was found to moult at least 18 times after metamorphosis (Ong 1966), suggesting it is an ideal model for the investigation of *CRT* expression related to moult cycles. In this study, a cDNA encoding *S. paramamosain* CRT was cloned and characterized. Accordingly, we examined its possible role in modulating crustacean Ca^{2+} homeostasis during the moult cycle.

Materials and methods

Experimental animals

The experimental animals, mud crabs in the developing stage, measuring 60–80 mm in carapace width, were obtained from Jiaxin, Zhejiang Province, China, in July of 2014. They were temporarily reared in a cement pool for at least 7 days before sacrificed, and cultured individually in plastic trays (0.3 × 0.2 × 0.2 m). And the crabs fed mussels every day. Water quality parameters was kept at 28 ± 1 C and 14 ± 0.3‰ salinity, based on their habitat and the photoperiod adjusted to 12 h light/dark. General health state was observed daily.

Observation of moult stages and sampling

Moult stages were determined based on the degree of setal development according to the method described by Drach & Tchernigovtzeff (1967), but with slightly modification. The maxlliped exopodite of *S. paramamosain* is sufficiently broad and transparent to allow accurate observation of the moult related setal development. Thus, it was used in this study. Briefly, the third maxilliped was carefully removed using a pair of scissors, placed on a clean glass slide. The epidermis of the third maxilliped and setae were then observed using a microscope (Nikon, Tokyo, Japan). Pictures were taken with 40× magnification using a microscope digital camera (Toupcam, Hangzhou, China) and images were analyzed accordingly. At least three moults per animal were recorded based on the morphology of setogenesis.

For all other experiments, male animals were used. Hepatopancreas and other tissues were taken from the crabs based on moult stages. Tissues were immediately placed in liquid nitrogen and kept at −80 C until required.

Identification and characterization of *SpCRT*

cDNA fragment amplification

Total RNA was extracted from hepatopancreas of *S. paramamosain* using RNAiso Plus (TaKaRa, Dalian, China) according to the manufacturer's protocol, and quantified by a NanoDrop 2000 spectrophotometer (Thermo Scientific, Wilmington, DE, USA). The template cDNA was reverse transcribed from total RNA using PrimeScript® RT reagent Kit (TaKaRa). The resulting cDNA samples were stored at −20 C until they were used as templates for conventional polymerase chain reaction (PCR) or real-time quantitative polymerase chain reaction (qPCR).

To obtain cDNA fragments of *SpCRT*, degenerate primers SpCRT-F and SpCRT-R were designed based on the highly conserved amino acid sequences of crustacean species [Genbank accession number: Chinese shrimp (*Fenneropenaeus chinensis*, ABC50166), giant tiger shrimp (*Penaeus monodon*, ADO00927)]. Degenerate PCR for *SpCRT* was performed and the PCR product was electrophoresed on an agarose gel, purified and cloned into a pMD19-T vector with a TA cloning kit (TaKaRa). The recombinant plasmids were transformed into trans 5α chemically competent cell of *Escherichia coli* (TaKaRa). The positive clones were screened by PCR with and then subsequently sequenced. And these resulting sequences were verified and subjected to cluster analysis in NCBI.

Rapid amplification of cDNA ends

Rapid amplification of cDNA ends (RACE)-Ready cDNA was synthesized from total RNA using the SMARTer™ RACE cDNA Amplification Kit (Clontech, Palo Alto, CA, USA). Both the 3′-cDNA ends and the 5′-cDNA end reaction conditions and components were performed according to the manufacturer's instructions. PCR products were isolated, purified, cloned and sequenced as described in the cDNA fragment amplification. Primers were listed in Table 1.

Bioinformatics analysis

The full-length cDNA sequence was identified by BLAST analysis in NCBI database (http://www.ncbi.nlm.nih.gov). The predicted amino acid sequence was determined using the EXPASY molecular biology server (http://web.expasy.org/blast/). SpCRT molecular mass and phosphorylation sites were predicted by ProtParam (http://web.expasy.org/protparam/) and NetPhos programs (http://www.cbs.dtu.dk/services/NetPhos/) respectively. Prediction of CRT domain repeats, motifs and features were performed using the simple modular architecture research tool (SMART; http://smart.embl-heidelberg.de/). N-glycosylation sites and putative signal peptide sequences were predicted at (http://www.cbs.dtu.dk/services/NetN-Glyc/) and (http://www.cbs.dtu.dk/services/SignalP/) respectively. Calreticulin family signature motifs were based on InterPro Scan (http://www.ebi.ac.uk/interpro/scan.html) predictions.

Multiple alignments of amino acid sequences of *S. paramamosain* CRT domains were performed using the ClustalX 1.81 software (http://www.clustal.org/) and edited by the GeneDoc software (http://www.psc.edu/biomed/genedoc). The

Neighbour-joining tree estimated from distances between the animal CRT amino acid sequences was built by Mega version 5.0 (http://www.megasoftware.net/), using P-distance and 1000 bootstrap (Tamura, Peterson, Peterson, Stecher, Nei & Kumar 2011). Deduced protein sequences of CRT from various species were retrieved from the GenBank (http://www.ncbi.nlm.nih.gov/genbank/).

Tissue distribution of *SpCRT* transcript

Total RNA from the different tissues including hemocytes, heart, hepatopancreas, gills, antennal gland, gut, muscle, hypodermis and thoracic ganglia of healthy crabs in inter-moult was isolated to investigate the tissue distribution of *SpCRT*. After cDNA were synthesized, the steady-state level of the *CRT* transcript was measured by real-time PCR using an SYBR® Advantage® qPCR Premix (TaKaRa). PCR primers for *SpCRT* gene and the *18S rRNA* reference gene (GenBank accession number: FJ774906) are shown in Table 1.

To validate the assay, PCR efficiency and specificity were assessed for both target and reference genes. Standard curves were constructed using 10-fold serial dilutions of the pooled hepatopancreas cDNA samples. The slope of each titration curve was used to calculate the amplification efficiency. To ensure amplification specificity, melting-curve analysis and agarose gel electrophoresis were conducted at the end of each PCR reaction.

For both target and reference genes, quantitative reverse transcription PCR was in triplicate assayed for the levels of *SpCRT* expression according to the manufacturer's protocol. The relative expression level of *SpCRT* in different tissues was determined by the comparative threshold cycle method ($2^{-\Delta\Delta Ct}$) (Wong & Medrano 2005). A representative value from hemocytes was used as the calibrator and all other quantities were expressed as an *n*-fold difference relative to calibrator.

Total calcium levels in the hepatopancreas

Samples for total calcium analysis were prepared using the method modified from Wilder, Do Thi Thanh, Jasmani, Jayasankar, Kaneko, Aida, Hatta, Nemoto & Wigginton (2009). Hepatopancreas samples were weighed and placed in a Petri dish for drying in an incubator at 110 C for at least 48 h until they reached a constant weight. Approximately, 1.0 g dry weight of each sample

Table 1 Primers used in this study

Primer name	Sequence 5′ → 3′
SpCRT-F	ATCTGYTCTGTKGGTYTGGA
SpCRT-R	CTCATCBTCMTCSTCYTCC
SpCRT-5′	GGGTGGGAGGGTTGAGGGGAAAGGGAC
SpCRT-3′ outer	GCATTGGAGACGAGACCTGGGGAG
SpCRT-3′ inner	GGATGAGGCCAAGAAGATGAAGGATGC
SpCRT real-F	AAGAGCCAGAACCACCTC
SpCRT real-R	CGTTGTCAATGAGCACCTCA
18S real-F	ACTCAACACGGGGAACCTCAC
18S real-R	CAAATCGCTCCACCAACTAAG

were mixed with 5 mL nitric acid and 2 mL of hydrogen peroxide were digested in a microwave oven (multiwave 3000; Anton Paar GmbH, Stuttgart, Germany) for over 2 h. The digests were then diluted with deionized water and external calibration curves were constructed for determining total calcium. The concentration of calcium was measured afterward using inductively coupled plasma of atomic emission spectroscopy (ICP-AES) technique (Optima8000; Perkin Elmer, Boston, MA, USA). The wavelengths used for Ca is 317.933 nm.

Determination of *SpCRT* transcript abundance during a moult cycle

To determine the hepatopancreas *SpCRT* transcription with the moult cycle, samples from different moult stages were determined using real-time PCR as described above.

Data presentation and statistical analysis

Statistical analyses were performed using Prism 5 software (GraphPad Software, La Jolla, CA, USA) with the minimum level of significance set to p 0.05. Data were examined using one-way ANOVA and followed by Tukey multiple comparisons tests. Data are expressed as mean ± standard error of the mean.

Results

SpCRT gene cloning and sequence analysis

The full-length cDNA of *SpCRT* (GenBank accession number: KP684144; Fig. 1) was 1699 bp long. It contained an open reading frame of 1221 bp encoding a polypeptide of 406 amino acids with the 5′ and 3′ UTRs of 40 and 421 bp respectively. The polyadenylation signal (AATAAA) was located at 16 bp upstream from the poly A tail.

Deduced amino acid sequence analysis of the SpCRT cDNA clone

The deduced SpCRT protein had a theoretical molecular weight and isoelectric point (pI) of 46.88 kDa and 4.32 respectively. The signal peptide (MKTWVFLALFGVALVES) was predicted to be cleaved between A17 and K18 (Fig. 1). The Net-Phos program predicted that SpCRT had 7, 5 and 10 putative phosphorylation sites for serine, tyrosine or threonine respectively. InterPro Scan analysis showed that SpCRT had two conserved calreticulin family signatures: KHEQNIDCGGGYLKVF (residues 96-111) and VMFGPDICG (residues 128–136) (Fig. 1). However, No Asn-linked glycosylation site was predicted. Similar to other crustacean CRTs, SpCRT had three evolutionarily conserved domains: N-, P- and C-domain (Fig. 2). The N-domain involved four of the histidine residues in this domain, four of five cysteine residues were found in the globular N-domain (Fig. 2). The N-domain was also enriched for six histidine residues; the P-domain, a highly conserved proline-rich region, extended from amino acid 199 to amino acid 312. This region contained three repeats of IXDPDXXKPXDWD (Fig. 1); Like CRT from various species, the C-terminus of CRT was enriched in negatively charged residues and ended with an HDEL sequence.

Multiple sequences and phylogenetic analysis

The SpCRT sequence was compared to several of the full-length CRT sequences found in the crustaceans. As shown in Fig. 2, the Clustal program revealed that the deduced amino acid sequence of SpCRT shared high identity with CRTs from *Cherax quadricarinatus* (89.14%), *F. chinensis* (88.02%), *Pacifastacus leniusculus* (87.22%), *P. monodon* (86.91%), *Palaemon carinicauda* (86.39%) and *Litopenaeus vannamei* (86.35%) respectively.

A phylogenic tree of SpCRT amino acid sequence and other species from animals was generated. Based on NJ analysis, a clear division was observed among vertebrates and invertebrates. In the invertebrates, all the CRTs clearly separated into two branches including insect and crustacea. SpCRT clustered with *P. leniusculus* CRT and allocated to be a member of crustacean CRTs (Fig. 3).

Tissue expression analysis of *SpCRT*

The spatial distribution of the *SpCRT* transcript was assessed by RT-PCR. The mRNA transcripts of *SpCRT* could be detected in all the examined tissues with different expression levels including hemocytes, thoracic ganglion, muscle, antennal gland, hepatopancreas, gills, gut, heart and hypodermis (Fig. 4). The highest expression level of *SpCRT* was found in hepatopancreas (p 0.05), while the lowest was in hemocytes.
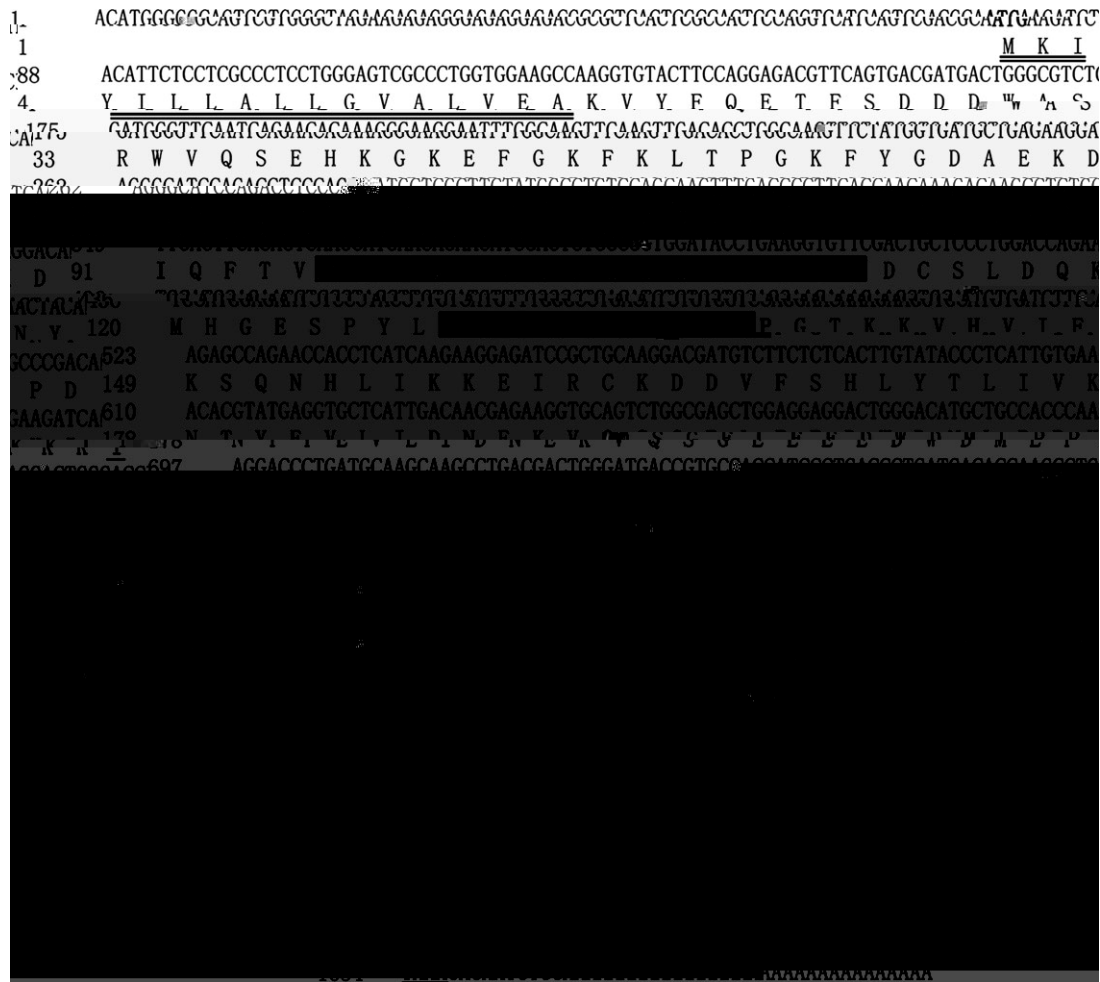
Figure 1 Nucleotide sequence of the *SpCRT* cDNA and its predicted amino acid sequence. Start and stop codons ( ) were in boldface. The predicted signal peptide was double-underlined. The two calreticulin family signature sequences were highlighted with grey box. Triplicate repeats (IXDXEXXKPE(/D)DWD) were marked with lines. The nuclear localization signal (HDEL) was white boxed. The polyadenylation signal (AATAAA) was underlined with bold line.

Moult staging

The moult cycle in *S. paramamosain* was divided into seven stages, termed early post-moult stage A, late post-moult stage B, inter-moult stage C, early pre-moult stage D_0 and middle pre-moult stage D_1, late pre-moult stage D_2 and moult stage E respectively. The morphological characteristics of these stages were studied in terms of setal development and epidermal retraction and invagination. Figure 5 shows a comprehensible and detailed chart with images of setal development of uropods in all moult stages of *S. paramamosain*.

Total calcium concentrations in hepatopancreas during the moult cycle

During the moult cycle, the total calcium concentrations in the hepatopancreas were measured using ICP-AES. The concentrations of total calcium were relatively lower at post-moult stage A (8.45 mg g^{-1}) and stage B (5.65 mg g^{-1}), which were significantly different from those levels at other moult stages (p 0.05, Fig. 6). Then it increased significantly at inter-moult stage C (13.42 mg g^{-1}) (p 0.05). At early pre-moult stage D_0 (17.10 mg g^{-1}), the quantity of calcium was similar to that of inter-moult (p 0.05); by
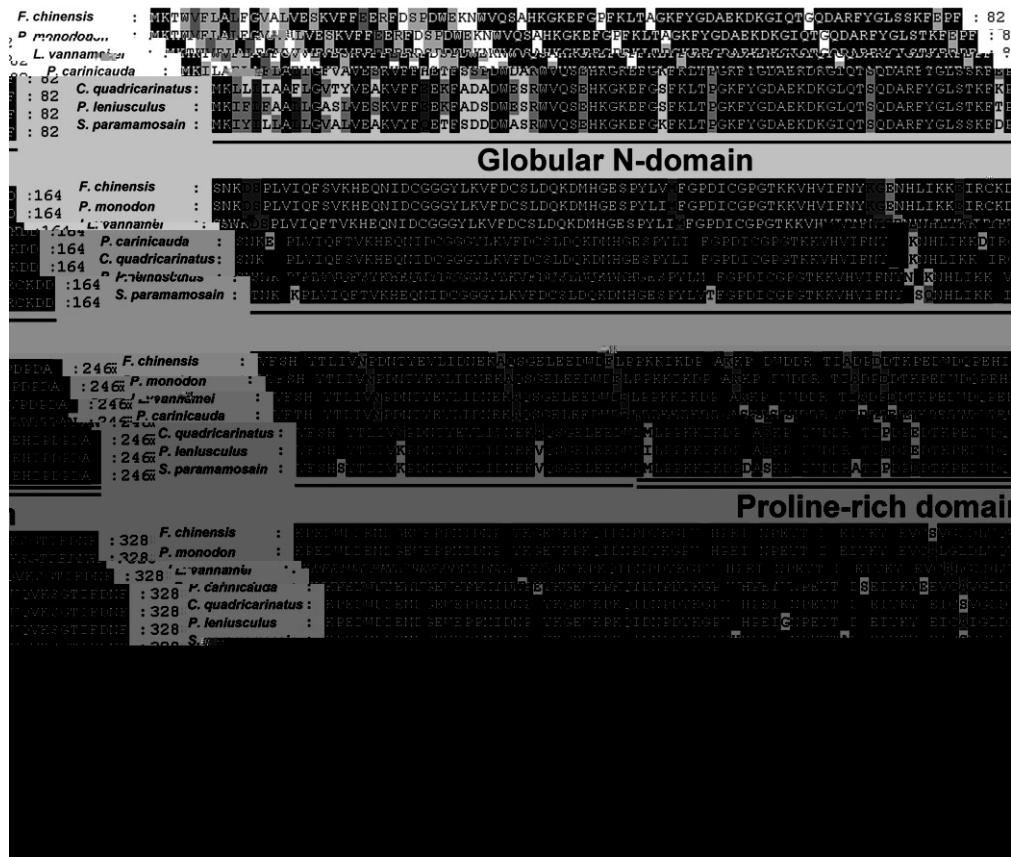
Figure 2 Alignment of the sequence of SpCRT with other CRTs from crustacean. Three domains were predicted in *Scylla paramamosain*. They were indicated with line, double-underline and dotted line respectively. Amino acids were numbered and sequences and accession numbers are shown for the following: *Fenneropenaeus chinensis* (ABC50166), *Penaeus monodon* (ADO00927), *Litopenaeus vannamei* (AFC34501), *Palaemon carinicauda* (AGJ03552), *Cherax quadricarinatus* (AIW68605), *Pacifastacus leniusculus* (AEC50079), *S. paramamosain* (KP684144).

early pre-moult stage D_1 (29.86 mg g^{-1}), calcium content was observed to begin increase significantly (p 0.05) until peaked at stage E (50.17 mg g^{-1}).

Expression analysis of *SpCRT* in crab at different moult stages

To better understand the possible roles of *SpCRT* in regulating the functional activity of hepatopancreas, we used real-time PCR to measure the relative abundance of the *SpCRT* transcript in hepatopancreas during the moult cycle of *S. paramamosain*. The results showed that different expression levels of *SpCRT* existed when crab were at different physiological state (Fig. 7). The level of *SpCRT* transcript in hepatopancreas was the lowest during moult (E) and post-moult (A), then it

increased significantly thereafter and maintained at a higher level at other stages (p 0.05). However, the highest expression level of *SpCRT* was detected at inter-moult (stage C) (p 0.05).

Discussion

This study describes the molecular cloning of a cDNA encoding a CRT from *S. paramamosain*. The protein family signatures, sequence alignment and phylogenetic analysis further confirmed that SpCRT was a member of the crustacean CRT family. Similar to CRTs from other species, several regions in their sequences are conserved. In the extremely conserved N-domain, the first and third cysteine residues could form a disulphide bridge (Cys^{103}-Cys^{135}), this bridge may be important for proper folding of the N-terminal region of
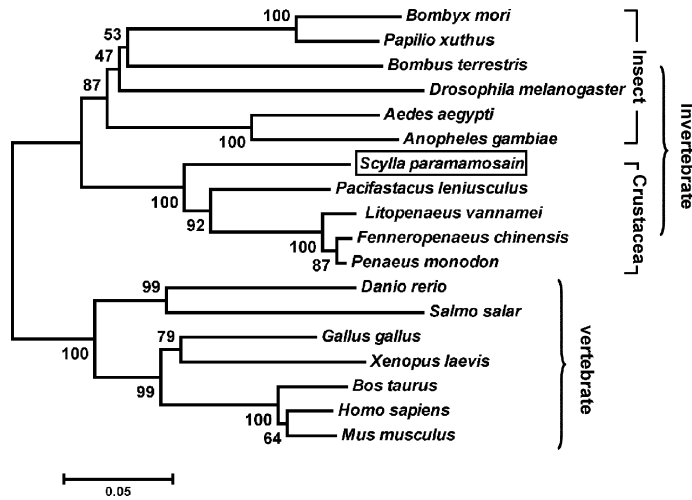
Figure 3 Phylogenetic analysis of the amino acid sequence of CRTs. Amino acid sequences of CRT from various species were collected from NCBI protein database. The numbers at the forks indicated the bootstrap. The protein sequences used for phylogenetic analysis were as follows: *Homo sapiens* (NP004334), *Bos Taurus* (NP76425), *Mus musculus* (NP031617), *Gallus gallus* (AAS49610), *Xenopus laevis* (CAA47866), *Danio rerio* (NP956007), *Salmo salar* (ACI33338), *Drosophila melanogaster* (NP524293), *Bombyx mori* (BAC57964), *Bombus terrestris* (XP003403200), *Anopheles gambiae* (AAL68781), *Aedes aegypti* (XP001657748), *Papilio xuthus* (BAM17778), *L. vannamei* (AFC34501), *F. chinensis*(ABC50166), *P. monodon* (ADO00927), *P. leniusculus* (AEC50079), *S. paramamosain* (KP684144).
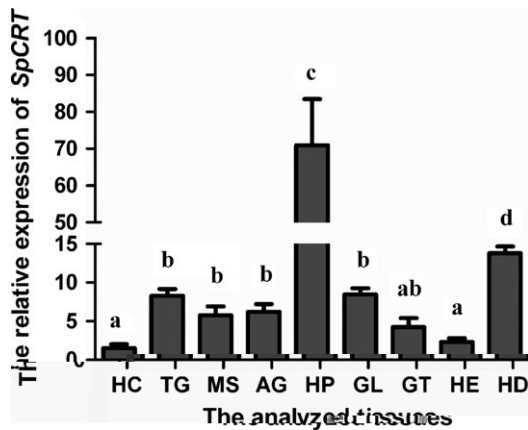

Figure 4 Distribution of the *SpCRT* mRNA transcript in inter-moult tissues of *Scylla paramamosain*. The reference gene is *18S rRNA*. HC, hemocytes; TG, thoracic ganglion; MS, muscle; AG, antennal gland; HP, hepatopancreas; GL, gills; GT, gut; HE, heart and HD, hypodermis. Vertical bars represent the mean ± SEM (n 7), Means with different superscript letters are significantly different at p 0.05 by the Tukey's HSD test.

calreticulin (Hojrup, Roepstorff & Houen 2001). However, no glycosylation of calreticulin was found in this region. It has been reported that the glycosylation of calreticulin is more common in plants than in animal cells (Michalak *et al.* 1999). In the P domain, this region contains three repeats IXDPDXXKPXDWD (Fig. 1). The function of binding-Ca^{2+} with low capacity, but relatively high-affinity in these motifs depends on the high percentage of acidic amino acids in this region. Moreover, this domain plays a regulatory role in the CRT lectin-like chaperone activity (Michalak *et al.* 2009). The C-terminus consist of many negatively charged residues, which may be crucial for binding Ca^{2+} with relatively high capacity, but low affinity. In addition, the terminated HDEL sequence is essential for targeting and retention of CRT in the ER lumen (Jia *et al.* 2009; Michalak *et al.* 2009).

In this study, *SpCRT* was widely expressed in various tissues of the crabs but with the highest in hepatopancreas. Hepatopancreas was not only regarded as the metabolic centre for reactive oxygen species production (Bianchini & Monserrat 2007) but also as a storage organ for calcium in crustacean (Greenaway 1985). Given the sequence features and the expression of *SpCRT* gene, it is reasonable to believe that it may play a general roles associate with Ca^{2+} homeostasis in hepatopancreas. Generally, the tissue distribution pattern of *SpCRT* transcript was similar that of *CRT* in other crustacean species, such as *F. chinensis*
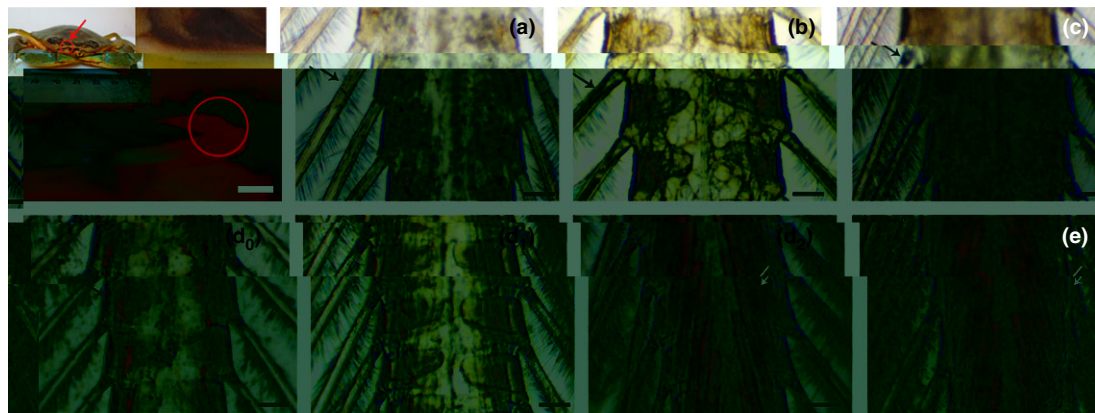
Figure 5 Morphological changes in setogenesis during moult cycle in juvenile *Scylla paramamosain*. The circle in the top left crab picture points the region of the third maxilliped used for setogenesis. From a to e: Stage a (early post-moult), arrow points to the setal lumen filled with setal matrix; Stage b (late post-moult), arrow shows retraction of the setal matrix (black one in setal lumen) and the beginning of internal cone formation; Stage c (intermoult), arrow reveals empty setal lumen, and the setal cone is formed; Stage d_0 (onset of pre-moult), arrows show the onset of the separation of the cuticle and epidermis (arrowheads); Stage d_1 (intermediate pre-moult), white arrow shows details of the newly formed setae; Stage d_2 (late pre-moult), arrow features new setae completely formed and folded under the old carapace; Stage e (moult), arrow show a gap between old carapace and new carapace, revealing crab is shedding off its old exoskeleton in ecdysis stage. All moult stage images are $40\times$, from 60 to 80 mm in carapace width animals. Scale bars: White: 1 mm, black: 0.1 mm.
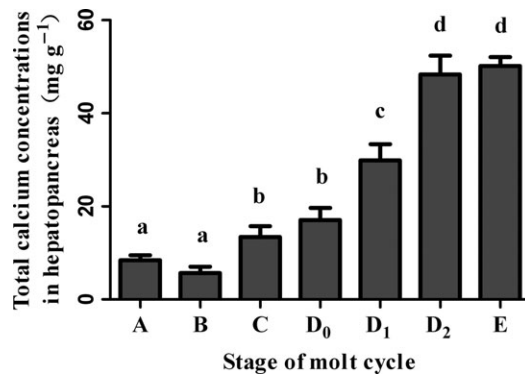

Figure 6 Changes in total calcium concentrations in the hepatopancreas of *Scylla paramamosain* during the moult cycle from stages A–E, (n 5); Data are presented as mean ± SEM (n 5), and the data with different letters are significantly different (Tukey's HSD test, $p < 0.05$).

Figure 7 Relative abundance of the *SpCRT* transcript in hepatopancreas during the moult cycle of *Scylla paramamosain*. A replicate from moult stage (E) was used as calibrator. Moult stages were moult (E), post-moult (A and B), inter-moult (C) and pre-moult (D_0–D_2). Bars represent mean ± SEM (n 7), means with different superscript letters are significantly different at p 0.05 by the Tukey's HSD test.

(Luana *et al.* 2007) and *Exopalaemon carinicauda* (Duan, Liu, Li, Wang, Li & Chen 2014).

To investigate the potential function of CRT in regulating Ca^{2+} homeostasis during the moult cycle, we first characterized the moult cycle of *S. paramamosain*. Setogenesis in *S. paramamosain* resembles that of the Dungeness crab *Cancer magister* (Drach & Tchernigovtzeff 1967) and *L.*
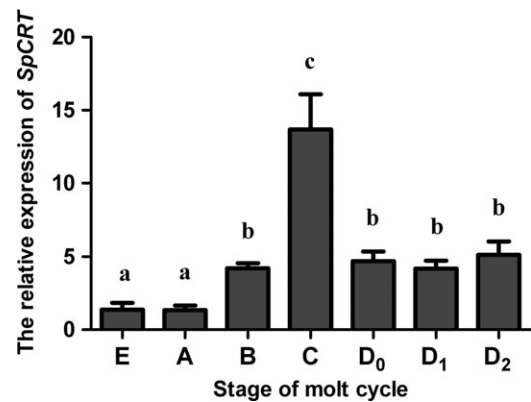
vannamei (de Oliveira Cesar, Zhao, Malecha, Ako & Yang 2006). In this study, setal cone formed at inter-moult phase in *S. paramamosain*. The formation of internal cone at the base of setae is also used to define the post-moult and inter-moult period (de Oliveira Cesar *et al.* 2006). However,

morphology of this structure varies considerably among families. This structure was not observed in basal endite of maxilla in snow crab (Moriyasu & Mallet 1986). Compared with moult stages in crustaceans have been determined by measurement of the histological examination of integument (Musgrove 2000) and regeneration of pereiopods (opaque in *S. paramamosain*) (Benhalima, Moriyasu & Hebert 1998), we provided a novel and practical methodology of determination of moult stages based on uropods of *S. paramamosain*.

We next found that the total calcium levels in hepatopancreas was relatively steady between inter-moult (stage C) and early pre-moult (stage D_0), subsequently increased to a peak till moult (stage E) and then fell sharply during post-moult (stage A and B) (Fig. 6). It was suggested that *S. paramamosain* exhibited calcium balance in inter-moult stage and stored calcium in hepatopancreas at middle and late pre-moult stage (stage D_1 and D_2) for calcifying the cuticle later after ecdysis. This result agrees with other studies on the Indian white prawn *Penaeus indicus* (Vijayan & Diwan 1996) and *L. vannamei* (Li & Cheng 2012). It is generally accepted that the hepatopancrealic cells play a considerable role in massive calcium transport between the exoskeleton and the hepatopancreatic storage sites during pre-moult and post-moult stages of crustaceans (Wheatly *et al.* 2002). Within the hepatopancreas cells, potential mechanism of calcium sequestration include attachment to calcium binding proteins (CRT and calmodulin), formation of $CaPO_4$/$CaSO_4$ granules and storage in intracellular organelles including ER and other organelles (Zilli, Schiavone, Storelli & Vilella 2007). And further studies will expand our understanding on the ratios of each calcium stores in the hepatopancreas of *S. paramamosain*.

Finally, quantitative real-time PCR results showed that the level of the *SpCRT* transcript in hepatopancreas was the lowest during stage E and A, increased significantly and remained higher in other stages (Fig. 7). In fact, together with the pattern of stage-specific changes in total calcium seen in hepatopancreas (Fig. 6), our result indicated that decreased calcium level at post-moult (stage A and B) in hepatopancreas cells was likely a consequence of down-regulation of *CRT* activity (stage E and A). Similarly, it was showed that the relatively higher expression of *SpCRT* in

hepatopancreas (compared with stage E and A) during pre-moult (stage D_1 and D_2) may be a cellular response designed to increase Ca^{2+} storage (Fig. 7). However, the lag between mRNA expression and the total calcium level might reflect the interval between nuclear mRNA transcription, translational regulatory processes and protein activation in the Golgi cisternae and ER. It is presumed that the *CRT* would remain somewhat higher for a certain duration until the moult (stage E), when again, changes would start occurring in preparation for the next moult. Thus, we concluded that *SpCRT* most likely plays Ca^{2+} homeostasis roles by increasing Ca^{2+} storage during the moult cycle. Up-regulation of calreticulin leads to increased amounts of Ca^{2+} in ER intracellular stores (Arnaudeau, Frieden, Nakamura, Castelbou, Michalak & Demaurex 2002), as the ER is the main Ca^{2+} storing organelle and over 50% of Ca^{2+} stored in the ER lumen is bound to calreticulin (Nakamura, Zuppini, Arnaudeau, Lynch, Ahsan, Krause, Papp, de Smedt, Parys, Muller-Esterl, Lew, Krause, Demaurex, Opas & Michalak 2001). Contrarily, calreticulin-deficient cells have reduced Ca^{2+}-storage capacity in the ER and delayed agonist-induced Ca^{2+} release (Guo, Lynch, Nakamura, Fliegel, Kasahara, Izumo, Komuro, Agellon & Michalak 2001; Michalak *et al.* 2009). However, inter-moult was associated with the greatest increase in *SpCRT* expression. Crustaceans spend most of their time in inter-moult, during this period they feed, reproduce and carry out day-to-day activities (Ahearn, Mandal & Mandal 2004). It is possible that besides the regulation of Ca^{2+} homeostasis, *SpCRT* gene products may play important roles in stress and immunity and other functions in this phase, as its multifunction had been confirmed in crustaceans (Luana *et al.* 2007; Visudtiphole, Watthanasurorot, Klinbunga, Menasveta & Kirtikara 2010; Duan *et al.* 2014). Nevertheless, further studies will be necessary to develop the homologous antibody to enable localization and quantification of expression of the CRT proteins.

In conclusion, seven moult stages of *S. paramamosain* were determined based on the setogenesis of the third maxilliped. Moreover, a full-length cDNA of CRT was cloned from *S. paramamosain*. A phylogenetic analysis suggests SpCRT is most closely related to the CRT proteins from other crustaceans. Tissue expression showed that expression of *SpCRT* was abundantly expressed in hepatopancreas. The expression of *SpCRT* and total calcium

variation in the hepatopancreas during the moult cycle suggested that *SpCRT* may play an important role in Ca^{2+} storage by regulating higher *SpCRT* expression. This research is essential for the elucidation of Ca^{2+} homeostasis mechanism in crustaceans during the more elusive stages.

Acknowledgments

References

Ahearn G.A., Mandal P.K. & Mandal A. (2004) Calcium regulation in crustaceans during the molt cycle: a review and update. *Comparative Biochemistry and Physiology, Part A* **137**, 247–257.

Arnaudeau S., Frieden M., Nakamura K., Castelbou C., Michalak M. & Demaurex N. (2002) Calreticulin differentially modulates calcium uptake and release in the endoplasmic reticulum and mitochondria. *Journal of Biological Chemistry* **277**, 46696–46705.

Benhalima K., Moriyasu M. & Hebert M. (1998) A technique for identifying the early-premolt stage in the male snow crab *Chionoecetes opilio* (Brachyura: Majidae) in Baie des Chaleurs, southern Gulf of St. Lawrence. *Canadian Journal of Zoology-Revue Canadienne De Zoologie* **76**, 609–617.

Bianchini A. & Monserrat J.M. (2007) Effects of methyl parathion on *Chasmagnathus granulatus* hepatopancreas: protective role of Sesamol. *Ecotoxicology and Environmental Safety* **67**, 100–108.

Bibi A., Agarwal N.K., Dihazi G.H., Eltoweissy M., van Nguyen P., Mueller G.A. & Dihazi H. (2011) Calreticulin is crucial for calcium homeostasis mediated adaptation and survival of thick ascending limb of Henle's loop cells under osmotic stress. *International Journal of Biochemistry and Cell Biology* **43**, 1187–1197.

Drach P. & Tchernigovtzeff C. (1967) Sur la me'thode de de'termination des stades d'intermue et son application ge'ne'rale aux Crustace's (in French with English abstract). *Vie Et Milieu Serie a-Biologie Marine* **18**, 595–610.

Duan Y., Liu P., Li J., Wang Y., Li J. & Chen P. (2014) Molecular responses of calreticulin gene to *Vibrio anguillarum* and WSSV challenge in the ridgetail white prawn *Exopalaemon carinicauda*. *Fish and Shellfish Immunology* **36**, 164–171.

Gao Y. & Wheatly M.G. (2007) Molecular characterization of an epithelial Ca^{2+} channel-like gene from crayfish *Procambarus clarkii*. *The Journal of Experimental Biology* **210**, 1813–1824.

Greenaway P. (1985) Calcium balance and molting in the crustacea. *Biological Reviews of the Cambridge Philosophical Society* **60**, 425–454.

Guo L., Lynch J., Nakamura K., Fliegel L., Kasahara H., Izumo S., Komuro I., Agellon L.B. & Michalak M. (2001) COUP-TF1 antagonizes Nkx2.5-mediated activation of the calreticulin gene during cardiac development. *Journal of Biological Chemistry* **276**, 2797–2801.

Hojrup P., Roepstorff P. & Houen G. (2001) Human placental calreticulin: characterization of domain structure and post-translational modifications. *European Journal of Biochemistry* **268**, 2558–2565.

Jia X.Y., He L.H., Jing R.L. & Li R.Z. (2009) Calreticulin: conserved protein and diverse functions in plants. *Physiologia Plantarum* **136**, 127–138.

Lenartowski R., Suwinska A. & Lenartowska M. (2015) Calreticulin expression in relation to exchangeable Ca^{2+} level that changes dynamically during anthesis, progamic phase, and double fertilization in Petunia. *Planta* **241**, 209–227.

Li C.H. & Cheng S.Y. (2012) Variation of calcium levels in the tissues and hemolymph of *Litopenaeus vannamei* at various molting stages and salinities. *Journal of Crustacean Biology* **32**, 101–108.

Luana W., Li F., Wang B., Zhang X., Liu Y. & Xiang J. (2007) Molecular characteristics and expression analysis of calreticulin in Chinese shrimp *Fenneropenaeus chinensis*. *Comparative Biochemistry and Physiology. Part B* **147**, 482–491.

Michalak M., Corbett E.F., Mesaeli N., Nakamura K. & Opas M. (1999) Calreticulin: one protein, one gene, many functions. *Biochemical Journal* **344**, 281–292.

Michalak M., Groenendyk J., Szabo E., Gold L.I. & Opas M. (2009) Calreticulin, a multi-process calcium-buffering chaperone of the endoplasmic reticulum. *Biochemical Journal* **417**, 651–666.

Moriyasu M. & Mallet P. (1986) Molt stages of the snow crab *Chionoecetes opilio* by observation of morphogenesis of setae on the maxilla. *Journal of Crustacean Biology* **6**, 709–718.

Musgrove R.J.B. (2000) Molt staging in the southern rock lobster *Jasus edwardsii*. *Journal of Crustacean Biology* **20**, 44–53.

Nakamura K., Zuppini A., Arnaudeau S., Lynch J., Ahsan I., Krause R., Papp S., de Smedt H., Parys J.B., Muller-Esterl W., Lew D.P., Krause K.H., Demaurex N., Opas M. & Michalak M. (2001) Functional specialization of calreticulin domains. *Journal of Cell Biology* **154**, 961–972.

de Oliveira Cesar J.R., Zhao B., Malecha S., Ako H. & Yang J. (2006) Morphological and biochemical changes in the muscle of the marine shrimp *Litopenaeus vannamei* during the molt cycle. *Aquaculture* **261**, 688–694.

Ong K.S. (1966) Observations on the post-larval life history of *Scylla serrata* reared in the laboratory. *Malaysian Agricultural Journal* **45**, 429–445.

Tamura K., Peterson D., Peterson N., Stecher G., Nei M. & Kumar S. (2011) MEGA5: molecular evolutionary genetics analysis using maximum likelihood, evolutionary distance, and maximum parsimony methods. *Molecular Biology and Evolution* **28**, 2731–2739.

Vijayan K.K. & Diwan A.D. (1996) Fluctuations in Ca, Mg and P levels in the hemolymph, muscle, midgut gland and exoskeleton during the molt cycle of the Indian white prawn, *Penaeus indicus* (Decapoda: Penaeidae). *Comparative Biochemistry and Physiology, Part A* **114**, 91–97.

Visudtiphole V., Watthanasurorot A., Klinbunga S., Menasveta P. & Kirtikara K. (2010) Molecular characterization of calreticulin: a biomarker for temperature stress responses of the giant tiger shrimp *Penaeus monodon*. *Aquaculture* **308**, S100–S108.

Wang W.A., Groenendyk J. & Michalak M. (2012) Calreticulin signaling in health and disease. *International Journal of Biochemistry and Cell Biology* **44**, 842–846.

Wheatly M.G., Zanotto F.P. & Hubbard M.G. (2002) Calcium homeostasis in crustaceans: subcellular Ca dynamics. *Comparative Biochemistry and Physiology, Part B* **132**, 163–178.

Wilder M.N., Do Thi Thanh H., Jasmani S., Jayasankar V., Kaneko T., Aida K., Hatta T., Nemoto S. & Wigginton A. (2009) Hemolymph osmolality, ion concentrations and calcium in the structural organization of the cuticle of the giant freshwater prawn *Macrobrachium rosenbergii*: changes with the molt cycle. *Aquaculture* **292**, 104–110.

Wong M.L. & Medrano J.F. (2005) Comment on Wong and Medrano's "Real-time PCR for mRNA quantification" – Response. *BioTechniques* **39**, 484–485.

Yeh S.P., Chiu C.H., Shiu Y.L., Huang Z.L. & Liu C.H. (2014) Effects of diets supplemented with either individual or combined probiotics, *Bacillus subtilis* E20 and *Lactobacillus plantarum* 7-40, on the immune response and disease resistance of the mud crab, *Scylla paramamosain* (Estampador). *Aquaculture Research* **45**, 1164–1175.

Zilli L., Schiavone R., Storelli C. & Vilella S. (2007) Analysis of calcium concentration fluctuations in hepatopancreatic R cells of *Marsupenaeus japonicus* during the molting cycle. *Biological Bulletin* **212**, 161–168.